Neurobiology of Disease

Adaptive Mossy Cell Circuit Plasticity after Status Epilepticus

Corwin R. Butler,[1] Gary L. Westbrook,[2] and Eric Schnell[1,3]

[1]Anesthesiology and Perioperative Medicine, Oregon Health & Science University, Portland, Oregon 97239, [2]Vollum Institute, Oregon Health & Science University, Portland, Oregon 97239, and [3]Portland VA Healthcare System, Portland, Oregon 97239

Hilar mossy cells regulate network function in the hippocampus through both direct excitation and di-synaptic inhibition of dentate granule cells (DGCs). Substantial mossy cell loss accompanies hippocampal circuit changes in epilepsy. We examined the contribution of surviving mossy cells to network activity in the reorganized dentate gyrus after pilocarpine-induced status epilepticus (SE). To examine functional circuit changes, we optogenetically stimulated mossy cells in acute hippocampal slices from male mice. In control mice, activation of mossy cells produced monosynaptic excitatory and di-synaptic GABAergic currents in DGCs. In pilocarpine-treated mice, mossy cell density and excitation of DGCs were reduced in parallel, with only a minimal reduction in feedforward inhibition, enhancing the inhibition/excitation ratio. Surprisingly, mossy cell-driven excitation of parvalbumin-positive (PV+) basket cells, primary mediators of feed-forward inhibition, was maintained. Our results suggest that mossy cell outputs reorganize following seizures, increasing their net inhibitory effect in the hippocampus.

Key words: **epilepsy; mossy cells; optogenetics; plasticity**

Significance Statement

Hilar mossy cell loss in epilepsy is associated with hippocampal hyperexcitability, potentially as a result of disrupted dentate microcircuit function. We used transgenic mice, translational mouse modeling, viral vectors, and optogenetics to selectively examine functional changes to mossy cell outputs following status epilepticus (SE). Interestingly, the outputs of surviving mossy cells exhibited adaptive plasticity onto target parvalbumin-positive (PV+) interneurons, resulting in a relative increase in their inhibitory control of dentate granule cells (DGCs). Our findings suggest that residual mossy cell outputs can reorganize in a homeostatic manner, which may provide clues for therapeutic targeting of this microcircuit.

Introduction

Structural and functional alterations of hippocampal circuits in temporal lobe epilepsy (TLE) manifest as imbalanced neuronal excitation and inhibition (Babb et al., 1984; Sloviter, 1987; Mello et al., 1993; Buckmaster and Dudek, 1997; Brooks-Kayal et al., 1998; Shibley and Smith, 2002; Nadler, 2003; Winokur et al., 2004). Several mechanisms likely contribute to this imbalance, including seizure-induced cell loss, circuit reorganization such as axon sprouting, and altered receptor expression (Sloviter, 1987; De Lanerolle et al., 1989; Brooks-Kayal et al., 1998; Shibley and Smith, 2002; Halabisky et al., 2010). However, it remains unclear whether the structural alterations that occur in hilar mossy cells contribute to hyperexcitability and thus disease progression, or involve adaptive modifications that maintain circuit homeostasis.

Glutamatergic hilar mossy cells give rise to bilateral long-range projections that drive direct excitation of dentate granule cells (DGCs) as well as feedforward inhibition of DGCs through local GABAergic interneurons (Scharfman, 1995; Hsu et al., 2016). Mossy cell projections are widely distributed in the hippocampus, suggesting that these cells broadly coordinate information transfer (Scharfman and Myers, 2013), and contribute to the essential role of the hippocampus in learning (Jinde et al., 2012; Bui et al., 2018). Mossy cells primarily receive excitatory and inhibitory input from neurons within the dentate gyrus and the CA3 pyramidal layer (Scharfman, 1994a, b, 2007; Williams et al., 2007; Larimer and Strowbridge, 2008; Sun et al., 2017), as well as from the lateral entorhinal cortex (Azevedo et al., 2019). The axons of mossy cells primarily target the inner molecular layer (IML) of the dentate gyrus (Buckmaster et al., 1996; Scharfman, 2016), albeit with projection differences between the dorsal and ventral hippocampus (Houser et al., 2020; Botterill et al., 2021a).

Received May 12, 2021; revised Feb. 1, 2022; accepted Feb. 6, 2022.

Author contributions: C.R.B., G.L.W., and E.S. designed research; C.R.B. performed research; C.R.B. analyzed data; C.R.B. wrote the first draft of the paper; C.R.B., G.L.W., and E.S. edited the paper; C.R.B., G.L.W., and E.S. wrote the paper.

This work was supported by the National Institutes of Health (NIH) Grant F32-NS106732 (to C.R.B.), the Department of Veterans Affairs Merit Review Awards I01-BX002949 (to E.S.) and I01-BX004938 (to E.S.), the Department of Defense Congressionally Directed Medical Research Program Award W81XWH-18-1-0598 (to E.S.), the NIH Grant R21-NS102948 (to Ines Koerner/E.S.), and the NIH Grant P30-NS061800 (Oregon Health & Science University Advanced Light Microscopy Core). We thank members of the E.S. and G.L.W. laboratories for critical feedback and discussion.

The authors declare no competing financial interests.

Correspondence should be addressed to Eric Schnell at schneler@ohsu.edu.

https://doi.org/10.1523/JNEUROSCI.1008-21.2022

As mossy cells are highly vulnerable to injury (Lowenstein et al., 1992; Zhang et al., 2015), alterations in mossy cell circuits after brain insults could profoundly alter hippocampal function (Santhakumar et al., 2000; Sloviter et al., 2003; Scharfman and Myers, 2013). For example, in the pilocarpine model of TLE, a large fraction of mossy cells are lost, while surviving mossy cells enlarge and receive increased excitatory input indicative of circuit reorganization (Zhang et al., 2015). The activation of residual mossy cells could either enhance or prevent seizures, depending on their net outputs, and thus result in different functional impacts for the circuit (Sloviter, 1991; Santhakumar et al., 2000; Sloviter et al., 2003; Botterill et al., 2019). Given these opposing possibilities, a functional understanding of mossy cell output connectivity after brain injury could elucidate their contribution to hippocampal function and excitability. However, selective activation of mossy cell axons has been challenging, as electrical stimulation in the IML can also activate semilunar granule cells, submammillary projections, and perforant path projections (Williams et al., 2007; Larimer and Strowbridge, 2008; Scharfman, 2016), as well as the extensive granule cell axon collaterals that sprout into the IML in epilepsy (Mello et al., 1993; Shibley and Smith, 2002; Winokur et al., 2004).

We combined genetic, viral, and anatomic methods to selectively target mossy cells with channelrhodopsin *in vivo*, to facilitate selective analysis of the mossy cell circuit three to four weeks after pilocarpine-induced status epilepticus (SE), which corresponds to an early stage of epileptogenesis in this model. We recorded mossy cell-evoked responses from granule cells and basket cells in acute slices from healthy mice and mice following pilocarpine-induced SE. Our results suggest that the net effect of the altered mossy cell circuit following SE is inhibitory.

Materials and Methods

Animals

Genetically modified male mice were used in experiments, beginning at six to eight weeks of age. We used only male mice because of the sex differences in the pilocarpine model of epilepsy, in which female mice are more resistant to pilocarpine induced SE (Buckmaster and Haney, 2012). Strains included calcitonin receptor-like receptor (Crlr)-Cre mice (The Jackson Laboratory #023014; Jinde et al., 2012) and Parvalbumin-IRES-Cre mice (The Jackson Laboratory #017320; Hippenmeyer et al., 2005) crossed with Rosa26-tdTomato marker mice (Ai14; The Jackson Laboratory #007914; Madisen et al., 2012), and maintained as homozygous colonies. For Parvalbumin-IRES-Cre::tdTomato mice, homozygous mice from each monogenic strain were bred to produce double heterozygotic offspring. Mice were housed in the Oregon Health & Science University vivarium, with food and water provided *ad libitum* and with a 12/12 h light/dark cycle. All procedures were approved by the Oregon Health & Science University Animal Care and Use Committee and followed the NIH *Guidelines for Care and Treatment of Animals*.

Cre-dependent viral vector delivery

To selectively label mossy cells in Crlr-Cre mice, we used unilateral intrahippocampal injections of a Cre-dependent adeno-associated virus (AAV) expressing an eYFP-tagged channelrhodopsin (pAAV-EF1a-double floxed-hChR2(H134R)-EYFP-WPRE-HGHpA, titer = 3.3×10^{13} cfu/ml, 20298-AAV5, Addgene), similar to a previous report (Bui et al., 2018). As our strategy to isolate mossy cell inputs onto parvalbumin-positive (PV+) cells involved Cre-expressing interneurons, we isolated mossy cell inputs in these mice by infecting commissural (contralaterally-projecting) mossy cells in PV-Cre::tdTomato mice with a non-Cre-dependent channelrhodopsin virus (pAAV-Syn-Chronos-GFP, titer = 5.3×10^{12} cfu/ml, 59170-AAV5, Addgene), similar to a previous report (Hsu et al., 2016). In these mice, subsequent electrophysiologic analysis was restricted to the contralateral (un-injected) hippocampus.

We performed intrahippocampal injections as previously described (Luikart et al., 2011), with injection coordinates targeting the dentate hilus (measured from bregma: +2.35 X, −2.80 Y, and −2.20 Z). One microliter of diluted viral stock (1:3 in sterile saline) was delivered at 0.25 µl/min using a calibrated Hamilton syringe (Hamilton; needle dimensions: 30 g, 0.5" length, 35° angle), with the needle remaining in place for at least 1 min following injection. All surgical procedures were performed under deep isoflurane anesthesia, and mice were provided soft food with oral acetaminophen solution following surgery. These injection parameters resulted in transduction of ChR2 in hilar mossy cells throughout most of the septo-temporal axis of the hippocampus, with a dense band of axonal ChR2-YFP expression in the IML of all sections/slices used for histologic or electrophysiological outcome measures. For each experiment, mice were injected with viral vectors two weeks before random allocation to either saline or pilocarpine injections, to control for differential infection of mossy cell cohorts between groups. Although we anticipate some variability in viral targeting between animals, we expect the average number of mossy cells labeled in each group before control or SE to have been the same.

Induction of SE

We used standard approaches to induce SE with pilocarpine as previously described (Shibley and Smith, 2002; Buckmaster and Haney, 2012; Zhang et al., 2015; Buckmaster et al., 2017; Hendricks et al., 2017). Briefly, two weeks following AAV injection, mice received an intraperitoneal injection of methyl-scopolamine (0.5 mg/kg, Sigma-Aldrich) 15–20 min before pilocarpine (325 mg/kg, i.p., Cayman Chemicals) or saline control. Following injection, mice were visually monitored for behavioral seizures, using a modified Racine scale to score seizure severity (Racine, 1972). Although studies vary in classification of SE, we identified mice as having achieved SE after three or more seizures with a Racine score of three or higher, followed by continuous stage 1–2 seizures (tremor, head bobbing, tail stiffening) for 2 h, consistent with established criteria (Shibley and Smith, 2002). After 2 h of SE, diazepam (10 mg/kg, i.p.) was administered to suppress seizure activity. Mice were then monitored, provided soft food, and received 1-ml warmed 5% dextrose solution in 0.45% saline twice daily (intraperitoneally) until they returned to normal behavior (1–3 d). Pilocarpine-injected mice that did not reach the criteria for SE were not used.

The initial injury severity of SE can be variable, with behavioral observations potentially missing subtle differences in seizure severities. Both the initial injury severity and subsequent development of spontaneous seizures can contribute to varied outcomes, including variable loss of hilar interneurons (Jiao and Nadler, 2007). To control for these variables, we used a standardized time spent in SE (2 h) in pilocarpine-treated mice, and a stage following status (three to four weeks post-SE) with lower incidence of spontaneous seizures, but this inherent variability in the model could contribute to variability in our data.

Slice preparation

Three to four weeks after pilocarpine-induced SE, mice were deeply anesthetized by isoflurane inhalation, injected intraperitoneally with 2% 2,2,2-tribromoethanol to maintain anesthesia, and decapitated while anesthetized. The brain was removed and placed in cold (2–4°C) oxygenated NMDG-based cutting solution containing the following: 93 mM NMDG, 30 mM $NaHCO_3$, 24 mM glucose, 20 mM HEPES, 5 mM Na-ascorbate, 5 mM *N*-acetyl cysteine, 3 mM Na-pyruvate, 2.5 mM KCl, 2 mM thiourea, 1.5 mM NaH_2PO_4, 0.5 mM $CaCl_2$, 10 mM $MgSO_4$, and 1 mM kynurenic acid equilibrated with 95% O_2-5% CO_2 (pH 7.2–7.4). Brains were blocked, glued to a sectioning stage, and slices (300 µm) were cut in the transverse plane into cold, oxygenated NMDG-based cutting solution using a vibrating microtome (Leica VT 1200S; Leica Biosystems). Slices were transferred to a storage chamber containing oxygenated NMDG-based solution at 32–34°C for 15 min, then transferred to a storage chamber at room temperature with oxygenated artificial CSF (ACSF) containing the following: 125 mM NaCl, 3 mM KCl, 2 mM $CaCl_2$, 1.25 mM NaH_2PO_4, 25 mM $NaHCO_3$, 1 mM $MgCl_2$, and 25 mM glucose. Slices of the hippocampus from hemispheres ipsilateral and contralateral to ChR2 virus injection were used in experiments from Crlr-Cre mice,

whereas only slices of the contralateral hippocampus from PV-Cre::tdT mice were used, and compared with slices from control mice that received scopolamine and saline injections. In Crlr-Cre experiments, data from ipsilateral and contralateral recordings were examined independently, producing qualitatively similar results, and pooled for analysis.

Whole-cell recordings

Transverse dentate gyrus hippocampal slices were transferred to a submerged recording chamber (Siskiyou PC-H) on an upright, fixed-stage microscope equipped with infrared, differential interference contrast optics (Olympus BX50WI), and continuously superfused with ACSF (2 ml/min). Recordings were performed at room temperature from visually identified DGCs, YFP-positive hilar mossy cells, or from parvalbumin-tdTomato-positive (PV-tdT+) basket cells in the subgranular zone (to selectively sample PV+ cells targeting granule cell somata; Ribak and Seress, 1983; Soriano and Frotscher, 1989; Vaden et al., 2020). For granule cell recordings, only granule cells in the outer half of the granule cell layer were patched, to avoid immature DGCs, which tend to be located near the subgranular zone, and semilunar granule cells, which are located in the molecular layer (Williams et al., 2007; Gupta et al., 2012; Save et al., 2019). All granule cells had whole-cell input resistances <1 GΩ. Recording pipettes were pulled from borosilicate glass (TW150F; World Precision Instruments) with a P-87 puller (Sutter Instruments). The intracellular solution for current clamp recordings contained the following: 130 mM KGluconate, 20 mM KCl, 10 mM HEPES, 0.1 mM EGTA, 4 mM MgATP, and 0.3 mM NaGTP. The intracellular solution for voltage clamp recordings contained the following: 113 mM CsGluconate, 8 mM NaCl, 10 mM EGTA, 10 mM HEPES, 1 mM $MgCl_2$, 1 mM $CaCl_2$, 3 mM CsOH, 2 mM MgATP, and 0.3 mM NaGTP. Open tip series resistance was 3–6 MΩ. Recordings were obtained using an Axopatch 1D amplifier (Molecular Devices), low-pass filtered at 10 kHz, digitized at 20 kHz with a NIDAQ (National Instruments) analog-to-digital board, and acquired using Igor Pro 5.05A (Wavemetrics) script with NIDAQmx (National Instruments) plugins. Cells were whole-cell voltage-clamped at −70 mV for 5–10 min to allow equilibration of pipette and intracellular solutions before data collection of light evoked responses. Cell series and input resistance were measured using a −10-mV voltage step (50 ms) before each sweep. The input resistance was calculated using V = IR, using the additional plateau (steady-state) current required to hold the −10-mV step after resolution of capacitive currents. Pulses of blue LED light (Thorlabs, 470 nm, 1 ms, 7.85 mW/cm^2) were delivered through a 40× water immersion objective above the YFP-positive hilar mossy cell (for mossy cell recordings) or above the IML for DGC or PV-tdT basket cell recordings, to optimally activate ChR2-expressing mossy cell axons. The $GABA_A$-receptor antagonist SR95531 (10 μM) was used to pharmacologically isolate excitatory synaptic input during optogenetic stimulation when indicated. Off-target expression can occur when using Cre-dependent viral vectors (Botterill et al., 2021c); however, our imaging demonstrated ChR2 expression was restricted to the hippocampus, and the pharmacologic sensitivity of optogentically-evoked responses was consistent with selective mossy cell activation. The di-synaptic nature of inhibitory currents during mossy cell evoked responses was confirmed by holding DGCs at the AMPAR reversal potential (0 mV) and applying the AMPAR-antagonist NBQX (10 μM), which eliminated the evoked inhibitory current at 0 mV as well as the evoked response at −70 mV (92.9 ± 1.13% block; $n = 8$ cells from 5 mice) leaving only a small residual (~6 pA) current completely insensitive to the $GABA_AR$ antagonist SR95531 (10 μM). AMPAR-mediated responses measured at −70 mV were short latency (<5 ms) with a smooth rise phase, suggesting minimal functional activation from the small number of observed infected CA3 cells, which could potentially activate DGCs via a di-synaptic pathway (Scharfman, 1994a). NMDA receptor (NMDAR)-mediated currents were recorded by holding DGCs at +40 mV to relieve magnesium block, and NMDAR-mediated current amplitudes were quantified 60 ms after optogenetic simulation, after decay of the AMPAR-mediated current.

Immunohistochemistry and imaging

To assess viral targeting, ipsilateral hemispheres from PV-Cre::tdT mice injected with AAV5-Syn-Chronos were removed at the time of contralateral acute slice preparation and drop-fixed in 4% paraformaldehyde (PFA) in PBS for 24–48 h at 4°C. For mice exclusively used for immunohistochemistry, terminally anesthetized mice (2% 2,2,2-tribromoethanol, 0.8 ml) were transcardially perfused with cold 0.1 M PBS followed by fixative containing 4% PFA in PBS. Brains were removed and postfixed (4% PFA in PBS) overnight at 4°C. The hippocampus was sectioned coronally (100 μm) using a Leica VT 1000S vibratome and three to four sections (600-μm interval between sections) were used for staining and imaging analysis. Sections were permeabilized with 0.4% Triton X-100 in PBS (PBS-T), blocked with 10% horse serum in PBS-T at room temperature for 1 h, and incubated in primary antibody [1:1000 goat anti-calretinin (CG1, SWANT; Schiffmann et al., 1999), 1:500 mouse anti-GAD67 (MAB5406, Sigma-Millipore; Varea et al., 2005), 1:500 guinea pig anti-ZnT3 (197-004, Synaptic Systems; Hendricks et al., 2017)] overnight at 4°C in 1.5% horse serum in PBS-T. Sections were rinsed with PBS and then incubated at room temperature for 4 h in PBS-T with 1:500 Alexa Fluor 488-conjugated rabbit anti-GFP (A21311, Invitrogen), 1:500 donkey anti-goat 647 (A21447, Invitrogen), 1:300 donkey anti-guinea pig 488 (706-545-148, Jackson ImmunoResearch), and 1:300 donkey anti-mouse 647 (A32787, Invitrogen) antibodies. The tdTomato signal in PV-Cre::tdT mice was bright and visualized without antibody enhancement. Tissue was counterstained with DAPI and mounted with Fluoromount G (SouthernBiotech) onto Fisher Superfrost slides (Fisher Scientific).

We acquired images for YFP+/tdT+ cells and ZnT3 labeling using either a Zeiss LSM 780 or LSM 900 laser scanning microscope on a motorized AxioObserver Z1 (Carl Zeiss MicroImaging). Zstack images (~15 μm) were collected with either a 5×, 20×, 40× (oil immersion), or 63× (oil immersion) objective. For CA3 pyramidal cell counts, we used an upright spinning disk confocal microscope (3i) to obtain single optical sections of DAPI-labeled CA3 cell nuclei in both hemispheres of two hippocampal slices per mouse, using 405-nm excitation with a 40× (oil immersion) objective. The Cell Counter plugin in FIJI (National Institutes of Health) was used to count cell densities. Imaging and quantification of cell densities were performed by an experimenter blinded to the experimental conditions. For CA3 cell density measures, we analyzed cells within a standardized area of 320 × 100 μm to compare cell counts within the pyramidal cell layer, to account for any decrease in CA3 pyramidal cell layer width between mice.

Data and statistical analysis

We used Igor Pro 5.05A (Wavemetrics) for curve fitting using an iterative least-squares method and evoked PSC analysis and GraphPad for additional statistical analysis. To quantify evoked responses,15–20 traces were averaged and measured for a given condition in each cell. Events characterized by a typical fast rise phase and exponential decay were selected for analysis. To compare the AMPAR/NMDAR ratio between cells, the peak AMPAR-mediated current amplitude at −70 mV was divided by the NMDAR-mediated current magnitude, measured from the combined evoked current at +40 mV, 60 ms after stimulation, when the AMPAR-mediated component had completely decayed to baseline (Hashimotodani et al., 2017). NMDAR-mediated currents were best fitted with a two exponential decay (fast and slow components; Tovar and Westbrook, 1999; Tovar et al., 2000), and a similar weighted decay was used to assess kinetics for these evoked currents. For all histologic and electrophysiology data, normality was tested using the Shapiro–Wilk test to determine use of parametric or nonparametric statistical analysis. Data were compared using a Student's t test for parametric outcome measures, whereas a Mann–Whitney U test was used for nonparametric data. Data are expressed as mean ± SEM, with significance set at $p < 0.05$. Sample sizes were selected to detect an effect size of 30–50% and a power of 0.8 with α set to $p < 0.05$.

Results

Reduced monosynaptic excitation of DCGs by mossy cells after SE

We combined *in vivo* injections of channelrhodopsin-expressing viral vectors with acute brain slice electrophysiology to analyze alterations in functional mossy cell-DGC connectivity three to four weeks after pilocarpine-induced SE. In this model, spontaneous seizures typically begin two to three weeks after SE (Mello et al., 1993; Shibley and Smith, 2002), followed by granule cell axon (mossy fiber) sprouting approximately one month after SE (Mello et al., 1993; Borges et al., 2003). We chose this time point to minimize polysynaptic activation of DGCs by sprouted mossy fibers (Hendricks et al., 2019). Under these conditions, single optogenetically-evoked EPSCs had sharp rise times, short latency, and low jitter, suggesting that recurrent activity was not contributing to our responses.

Crlr-Cre mice express Cre recombinase in hilar mossy cells of the hippocampus, with some expression in proximal CA3 cells (Jinde et al., 2012). When crossed with Rosa26-tdTomato reporter mice (Ai14), our preliminary analysis revealed significant off-target Cre-mediated recombination in pyramidal cells widely throughout CA3, as well as in Purkinje cells of the cerebellum. Thus, we used direct hilar injections of Cre-dependent viruses to selectively express ChR2 in mossy cells. In control mice, there was widespread ipsilateral ChR2-YFP expression in hilar mossy cells (72.8 ± 4.4% of calretinin-positive cells co-labeled with ChR2-YFP; $N = 4$ control mice), with a dense band of bilateral IML ChR2-YFP expression in all slices and sections used in this study, corresponding to mossy cell axonal projections (Fig. 1*A*,*B*). As per the original report (Jinde et al., 2012), in some sections we observed a small number of infected CA3 cells near the injection site. We also observed that a small number of mossy cells were sometimes labeled in the contralateral hilus, perhaps via axonal transduction (Burger et al., 2004; Castle et al., 2014) or ventricular viral spread. ChR2-YFP-expressing cells were never observed outside of the hippocampus. ChR2-YFP expression was not observed in GAD+ hilar interneurons or DGCs (data not shown).

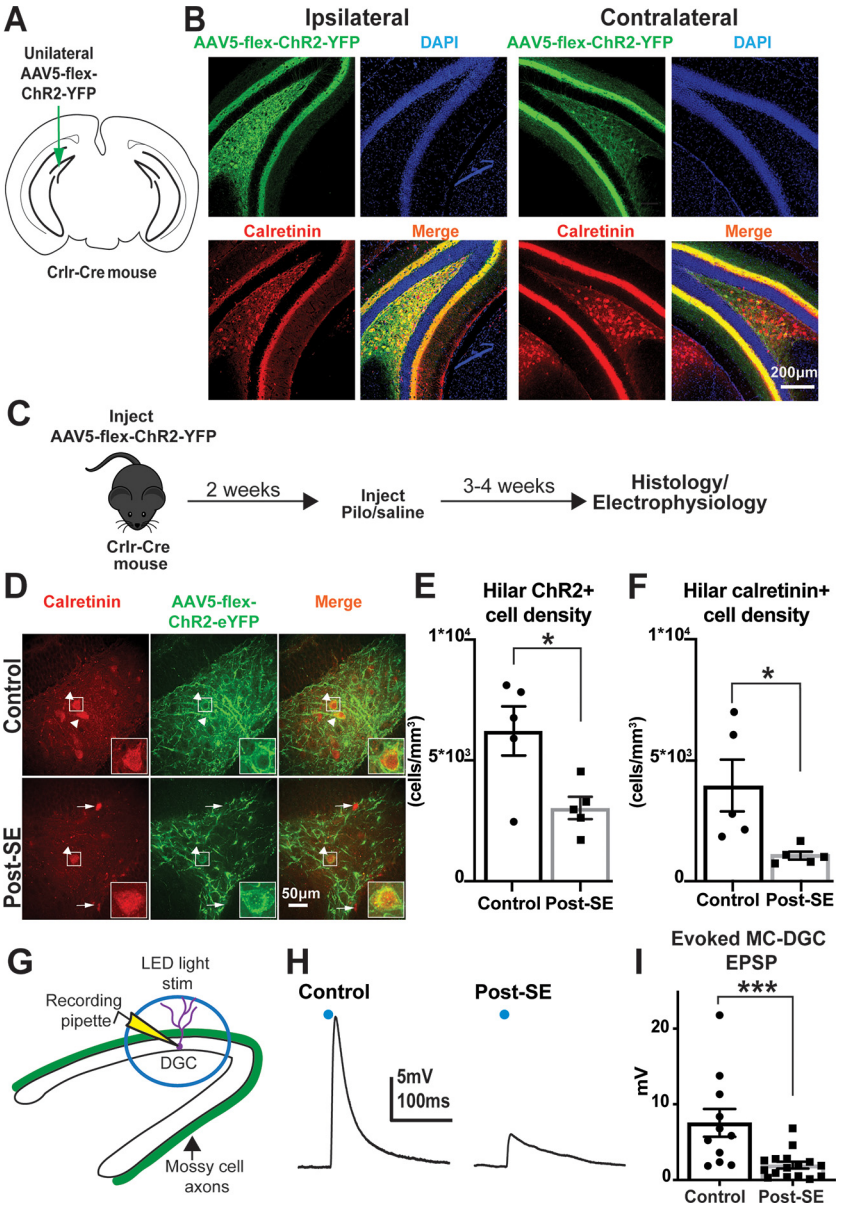

Figure 1. Mossy cell loss after SE reduces their excitation of DGCs. ***A***, Schematic of experimental design involving unilateral injection of AAV5-flex-ChR2-YFP virus into the dentate hilus of Crlr-Cre mice. Transduction of ChR2+ hilar mossy cells appeared throughout the septo-temporal axis of the ipsilateral hippocampus with a small number of contralateral hilar cells and ipsilateral CA3 pyramidal neurons. ***B***, Representative image of ipsilateral and contralateral ChR2-YFP expression (green), which labels calretinin expressing mossy cells (red) in the ipsilateral hilus and forms dense ipsilateral and contralateral IML projections, consistent with mossy cell axon innervation. Nuclear stain (DAPI, blue) also shown. ***C***, Experimental timeline, in which virus is injected two weeks before pilocarpine-induced SE or saline injections. ***D***, Representative images of ChR2-YFP and calretinin expression in control and post-SE mice, three weeks after saline/pilocarpine injections. Mossy cells are identified by their hilar location and size (arrowheads), as distinct from small calretinin-positive adult born neurons (arrows), which localize primarily to the subgranular zone and granule cell layer, and are increased after SE (lower images). ***E***, Hilar ChR2+ cell density is reduced in post-SE mice (*$p < 0.05$, unpaired t test). ***F***, Hilar calretinin+ cell densities (*$p < 0.05$, unpaired t test) from control and post-SE mice not injected with virus, also demonstrating mossy cell loss after SE. ***G***, Schematic illustrating DGC recording configuration during acute slice experiments, and optogenetic activation of mossy cell axons. ***H***, Representative recordings of optogenetically-evoked EPSPs in DGCs from control or post-SE tissue. ***I***, Mossy cell-evoked EPSP amplitudes obtained in DGCs from control and post-SE mice (***$p < 0.001$, Mann–Whitney).

ChR2+-labeled mossy cell density was reduced following pilocarpine-induced SE (control = 6220 ± 1020 cells/mm^3, $N = 5$ mice; post-SE = 3030 ± 460, $N = 5$ mice: unpaired t test, $t_{(8)} = 2.853$, $p = 0.0214$; Fig. 1*D*,*E*), consistent with hilar mossy cell loss (Zhang et al., 2015). Mossy cell loss was not related to viral injection, as calretinin labeling was also reduced after pilocarpine-induced SE in noninjected animals (control = 3590 ± 980 cells/mm^3, $N = 5$ mice; post-SE = 1040 ± 340, $N = 5$ mice: unpaired t test, $t_{(8)} = 2.568$, $p = 0.0332$; Fig. 1*F*). Although calretinin tends to preferentially label the more ventral mossy cell population (Houser et al., 2020; Botterill et al., 2021a), our dual

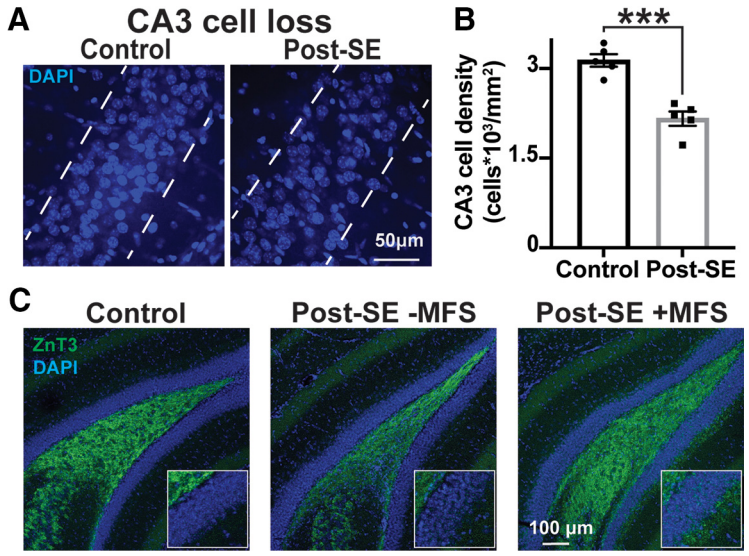

Figure 2. Histopathologic changes three to four weeks after SE injury. ***A***, Representative high magnification images of CA3 cell nuclei (as revealed by DAPI staining) in sections from control and post-SE mice (white dashed lines indicate the CA3 cell body layer boundaries). ***B***, CA3 cell loss in post-SE mice (***$p < 0.001$, unpaired t test). ***C***, Mossy fiber terminal labeling (ZnT3, green) in control and post-SE mice, qualitatively demonstrating small amounts of mossy fiber sprouting (MFS) in some mice. Magnification of granule cell and IML in insets.

observations of both decreased calretinin-positive and YFP-positive cells are consistent with many prior observations of mossy cell loss after pilocarpine-induced SE (Jiao and Nadler, 2007; Zhang et al., 2015; Bui et al., 2018).

To examine direct excitatory activation of DGCs by mossy cells, we measured the EPSPs evoked by optogenetic stimulation of ChR2-expressing mossy cell axons in whole-cell current clamp in the presence of the $GABA_AR$ antagonist SR95531 (10 μM). In prior reports, optogenetic stimulation of sprouted DGC axons in pilocarpine-treated mice caused multipeak evoked responses in recorded DGCs, because of the recurrent activation of neighboring granule cells (Hendricks et al., 2019). However, in our experiments, optogenetic stimulation of mossy cells reliably triggered single peak, short latency EPSPs in DGCs in both control and post-SE mice, indicating that evoked responses were from mossy cell axons and not from recurrent excitatory inputs from DGC axons that sprouted after SE. Mossy cell-evoked EPSPs were markedly reduced in DGCs from post-SE mice compared with control DGCs [control = 7.55 ± 1.83 mV, $n = 11$ cells (7 mice), post-SE = 1.96 ± 0.44 mV, $n = 16$ cells (6 mice); Mann–Whitney, $p = 0.0006$; Fig. 1*G–I*]. The latency to depolarization (10% rise time) was not affected (control = 3.40 ± 0.17 ms, post-SE = 3.54 ± 0.14 ms, $t_{(25)} = 0.61$, $p = 0.55$). The reduction in EPSP amplitude paralleled the reduced mossy cell density after SE, suggesting that the reduction in EPSP amplitude could be attributed to the loss of functional innervation resulting from mossy cell loss.

Loss of hilar interneurons and CA3 pyramidal neurons typically occurs in the first days after SE, while axon reorganization often requires a few weeks to develop, in parallel with the onset of variable spontaneous behavioral seizures (Shibley and Smith, 2002; Borges et al., 2003; Buckmaster et al., 2017). To help contextualize the relative time point of our analysis within disease progression after SE, we examined tissue sections to assess some of the histopathological features associated with epileptogenesis in our model: CA3 neuron loss and DGC axon (mossy fiber) sprouting. At this experimental time point, we observed consistent loss of CA3 neurons in post-SE mice relative to controls (control = 3130 ± 110 cells/mm^2, $N = 5$ mice; post-SE = 2160 ± 120 cells/mm^2, $N = 5$ mice; unpaired t test, $p = 0.0003$; Fig. 2*A*,*B*) and variable mossy fiber sprouting (three of the five post-SE mice had detectable zinc transporter 3 (ZnT3) staining in the granule cell layer and/or IML; Fig. 2*C*), consistent with the three- to four-week post-SE time point representing an early phase in epileptogenesis.

The reduced light-evoked EPSP was not because of diminished optogenetic activation of surviving mossy cells, as surviving mossy cells in post-SE mice reliably responded to light pulses with single action potentials as did ChR2+ mossy cells in control mice (Fig. 3*A–C*). Input resistance was also unaltered in surviving mossy cells (control = 128 ± 28 MΩ, post-SE = 123 ± 18 MΩ, unpaired t test, $t_{(16)} = 0.15$, $p = 0.89$). However, after SE, mossy cells had an increased frequency of spontaneous EPSPs [sEPSPs; control = 3.77 ± 0.77 Hz, $n = 7$ cells (5 mice); post-SE = 9.91 ± 1.17 Hz, $n = 7$ cells (6 mice); $t_{(12)} = 4.388$; $p = 0.0009$, unpaired t test; Fig. 3*D*,*E*], similar to previous reports (Zhang et al., 2015) without an effect on sEPSP amplitude [control = 2.08 ± 0.30 mV, $n = 7$ cells (5 mice); post-SE = 2.05 ± 0.26 mV, $n = 7$ cells (6 mice); unpaired t test, $t_{(12)} = 0.089$, $p = 0.93$]. However, the increase in sEPSPs was not associated with increased spontaneous firing of mossy cells in our slice preparation [control = 0.38 ± 0.17 Hz, $n = 8$ cells (5 mice); post-SE = 0.46 ± 0.17 Hz, $n = 9$ cells (5 mice); unpaired t test, $t_{(15)} = 0.336$, $p = 0.74$]. Additionally, we did not observe spontaneous mossy cell bursting (≥3 action potentials on a single sEPSP) in either group, nor did we observe increased bursting in response to optogenetic depolarization or current injection into ChR2-YFP+ mossy cells (data not shown).

Functional properties of mossy cell-DGC synapses after SE

To gain further insights into the network consequences of mossy cell loss after SE, we examined the properties of excitatory synapses from mossy cells onto DGCs using voltage-clamp recordings. As would be expected from the reduced optogenetically-evoked potentials (Fig. 1*F–H*), optogenetically-evoked mossy cell EPSCs were also reduced in DGCs in post-SE mice [AMPAR-mediated EPSC; control = 45.9 ± 9.6 pA, $n = 21$ cells (8 mice), post-SE = 19.6 ± 5.1 pA, $n = 21$ cells (9 mice); Mann–Whitney, $p = 0.0067$; Fig. 4*B*,*D*]. NMDAR-mediated EPSCs, recorded at a holding potential of +40 mV, were similarly reduced in post-SE DGCs (control = 29.7 ± 5.2 pA, $n = 16$ cells, post-SE = 12.6 ± 4.9, $n = 13$ cells; Mann–Whitney, $p = 0.0048$; Fig. 4*B*,*E*). There was no difference in the AMPAR/NMDAR ratio between groups (control = 1.37 ± 0.16, post-SE = 1.24 ± 0.20; Mann–Whitney, $p = 0.57$; Fig. 4*F*), indicating that there were no significant changes in the receptor complement at mossy cell-DGC excitatory synapses after SE. Both series resistance and input resistance of target DGCs were similar between groups (input resistance: control = 398 ± 46 MΩ, post-SE = 487 ± 56 MΩ, $t_{(40)} = 1.24$, $p = 0.22$; series resistance: control = 15.1 ± 1.3 MΩ, post-SE = 17.6 ± 1.8 MΩ, $t_{(40)} = 1.17$, $p = 0.25$), indicating that differences in these passive membrane properties did not contribute to the reduced AMPAR-mediated input in DGCs from post-SE mice.

Mossy cell-DGC EPSC rise and decay kinetics were also unaffected by SE (AMPA 10–90% rise-time: control = 3.53 ± 0.35 ms, post-SE = 3.25 ± 0.28 ms, Mann–Whitney, $p = 0.88$; AMPA

decay tau: control = 7.62 ± 0.39 ms, post-SE = 8.09 ± 0.63 ms, Mann–Whitney, $p = 0.78$; NMDA weighted decay: control = 177 ± 14 ms, post-SE = 163 ± 16 ms, $t_{(23)} = 0.64$, $p = 0.53$). Additionally, paired pulse stimulation revealed similar paired pulse depression at mossy cell-DGC synapses in post-SE mice and controls (100-ms interstimulus interval: control = 0.75 ± 0.06 P2/P1 ratio, $n = 14$ cells, post-SE = 0.84 ± 0.10 P2/P1 ratio, $n = 14$ cells; Mann–Whitney, $p = 0.95$; Fig. 4*G–I*). Together, these results suggest that reduction in population EPSC amplitudes at mossy cell-DGC synapses could be largely attributed to a decrease in the number of mossy cells, but that surviving mossy cell-DGC excitatory synapses have typical presynaptic and postsynaptic properties.

Mossy cell-driven output favors feedforward inhibition of DGCs after SE

Di-synaptic feedforward inhibition of DGCs by mossy cells is a prominent component of the dentate mossy cell circuit (Hsu et al., 2016; Scharfman, 2016). In addition to reduced excitation of DGCs, mossy cell loss could reduce excitation of interneurons, and thus also reduce feedforward inhibition. Therefore, we optogenetically stimulated mossy cells to examine di-synaptic $GABA_A$R-mediated IPSCs. Despite a substantial reduction in the mossy cell-driven AMPAR-mediated current after SE (57% decrease, Fig. 4*D*), there was a smaller reduction (44%) in the feedforward GABAergic input from mossy cells onto DGCs that barely reached significance [control = 41.8 ± 9.6 pA, $n = 21$ cells (8 mice), post-SE = 23.3 ± 6.4 pA, $n = 21$ cells (9 mice); Mann–Whitney, $p = 0.049$; Fig. 5*B*,*C*]. When examined on a cell-by-cell basis, the ratio of inhibition to excitation (I:E ratio) driven by mossy cell activation was significantly increased after SE (GABAR/AMPAR-mediated amplitude; control = 1.77 ± 0.58, post-SE = 3.42 ± 1.27; Mann–Whitney, $p = 0.015$; Fig. 5*D*). Thus, although both direct and indirect connectivity to DGCs was reduced after SE, there was relative preservation of the di-synaptic inhibitory output from surviving mossy cells onto DGCs, shifting the net synaptic output of mossy cells toward greater inhibition of DGCs.

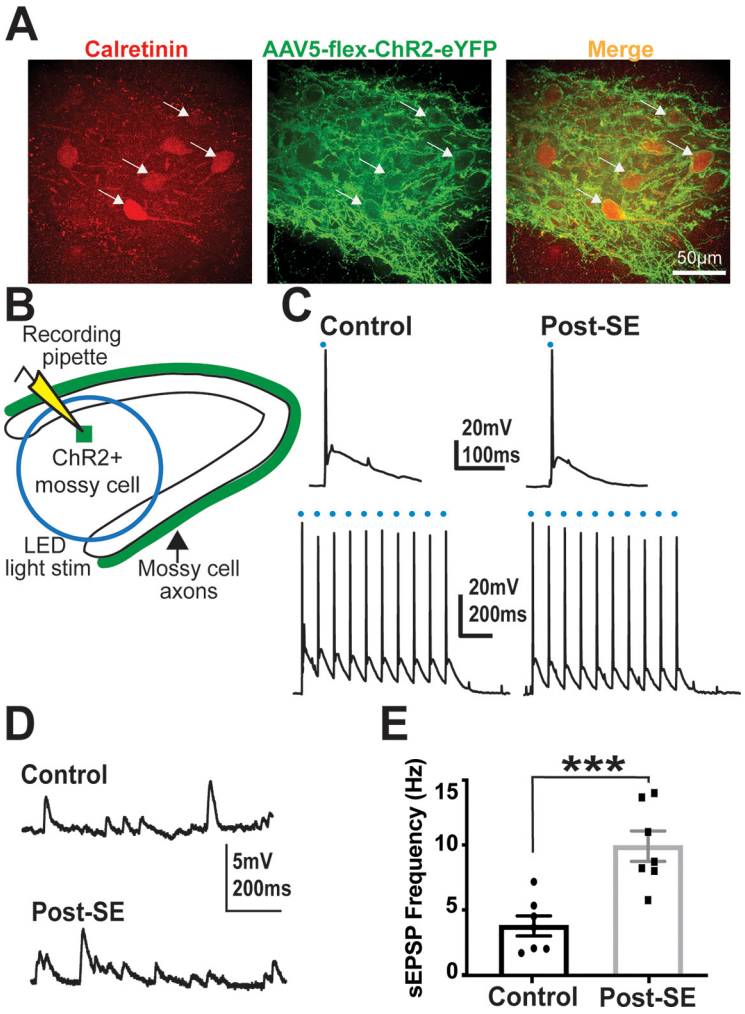

Figure 3. Characterization of ChR2-expressing mossy cells in control and post-SE mice. ***A***, Representative high magnification images of ChR2+ hilar cells (green), co-labeled (arrows) with calretinin (red). ***B***, Schematic of recording setup. ***C***, LED-evoked action potentials in ChR2+ mossy cells after single pulses or 10-Hz trains of 1-ms light stimulation, demonstrating similar activation of cells from control and post-SE mice. ***D***, Representative sEPSP recordings from ChR2+ mossy cells from control and post-SE mice in the absence of light stimulation. ***E***, ChR2+ mossy cells from post-SE mice have an increased sEPSP frequency relative to controls (***$p < 0.001$, unpaired *t* test).

Mossy cell-mediated input to PV+ basket cells is preserved after SE

Commissural projecting neurons in the hippocampus, which includes mossy cells, provide substantial synaptic input onto PV+ basket cells, primary mediators of feedforward inhibition, and to a lesser extent other interneuron populations in the dentate (Hsu et al., 2016). PV+ basket cells reside within the subgranular zone of the dentate gyrus (Ribak and Seress, 1983; Soriano and Frotscher, 1989; Vaden et al., 2020), and receive excitatory innervation from mossy cells, as well as from semilunar DGCs and medial entorhinal fibers (Hsu et al., 2016; Rovira-Esteban et al., 2020). Because of the importance of PV+ basket cells in mediating feedforward inhibition of DGCs, we examined the mossy cell to PV+ basket cell circuit as a potential site of plasticity for the relative preservation of di-synaptic inhibitory mossy cell output after SE. To label PV+ basket cells for slice recording experiments, we crossed a PV-specific Cre driver line mouse (Hippenmeyer et al., 2005) with a tdTomato reporter mouse line, to identify these cells for subsequent recording.

Consistent with prior immunohistochemistry in epileptic rodent brain (Buckmaster and Dudek, 1997; Wittner et al., 2001), we did not observe a change in PV+ basket cell density following pilocarpine-induced SE (control = 602.9 ± 121.8 PV-tdT+ cells/mm^3, $N = 13$ mice, post-SE = 535.1 ± 127.4 PV-tdT+ cells/mm^3, $N = 9$ mice; $p = 0.60$, Mann–Whitney; Fig. 6*A*, *B*). Following SE, PV+ cells also showed no differences in sEPSC amplitude and frequency (amplitude: control = 33.5 ± 3.4 pA, $n = 11$ cells/7 mice, post-SE = 29.5 ± 3.9 pA, $n = 8$ cells/6 mice; $t_{(17)} = 0.777$; $p = 0.45$, unpaired *t* test; frequency: control = 3.23 ± 0.74 Hz, $n = 11$ cells/7 mice, post-SE = 4.99 ± 1.61 Hz, $n = 8$ cells/6 mice; $p = 0.35$, Mann–Whitney; Fig. 6*C–E*), indicating that these interneurons are present in normal number and maintain excitatory input after SE-induced reduction in the number of mossy cells.

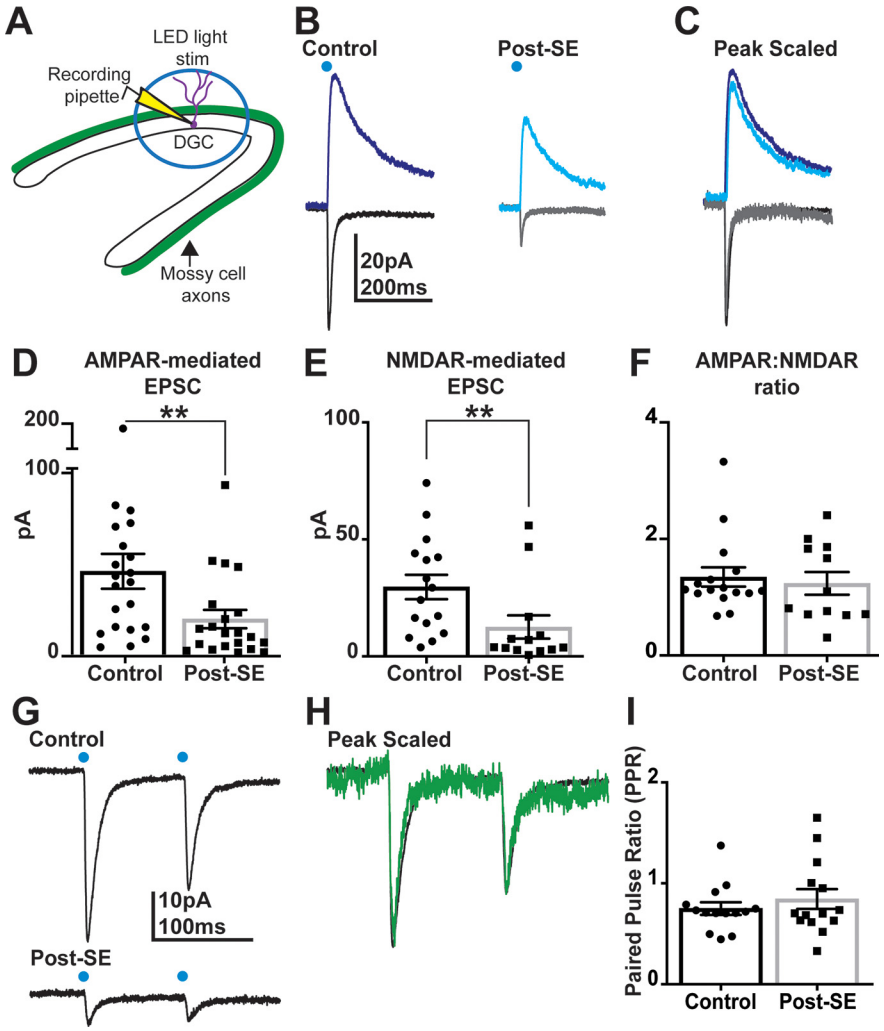

Figure 4. Mossy cell loss after SE does not alter receptor composition or short-term plasticity of remaining mossy cell-DGC synapses. ***A***, Schematic illustrating DGC recording configuration during optogenetic activation of mossy cell axons. ***B***, Representative EPSCs in DGCs resulting from mossy cell activation in control and post-SE mice. The black trace was recorded at −70 mV (AMPAR-mediated) and the blue trace was recorded at +40 mV (AMPAR-mediated and NMDAR-mediated), both with $GABA_A$ receptors blocked. ***C***, Peak-scaled responses (to AMPAR-EPSC peak; light colored traces from post-SE mice) in control and post-SE conditions. ***D***, Summary data showing light-evoked AMPAR-mediated response amplitudes in DGCs from control and post-SE mice (**$p < 0.01$, Mann–Whitney). ***E***, Summary data showing light-evoked NMDAR-mediated response amplitudes in DGCs from control and post-SE mice (**$p < 0.01$, Mann–Whitney). ***F***, The ratio of AMPAR:NMDAR-mediated response amplitudes is unchanged after SE ($p = 0.57$, Mann–Whitney). ***G***, Representative currents evoked by paired-pulse stimulation (100-ms interval) in DGCs from control and post-SE mice. ***H***, Peak-scaled paired-pulse responses from ***G*** (green trace from post-SE mice). ***I***, Paired pulse ratio is unchanged for mossy cell-evoked responses in DGCs from control versus post-SE mice ($p = 0.95$, Mann–Whitney).

To selectively examine the mossy cell-mediated input to PV+ basket cells, we unilaterally injected the dentate hilus of PV-Cre:: tdT mice with a non-Cre-dependent channelrhodopsin virus (AAV5-Syn-Chronos-GFP), to target commissural projections of mossy cells to the contralateral dentate gyrus. This resulted in the expected widespread infection of cells throughout the dentate gyrus in the ipsilateral hemisphere, but more importantly allowed us to selectively stimulate mossy cell inputs in slices from the contralateral hemisphere while recording from genetically identified (tdTomato+) PV+ basket cells. Chronos-GFP expression in the contralateral hippocampus was restricted to mossy cell axons in the IML (Fig. 7*A*,*B*). Two weeks after virus injection and mossy cell labeling, mice were randomized to either control or pilocarpine-mediated SE. At the same early time point (three to four weeks after SE), acute hippocampal slices were prepared to examine the connectivity of mossy cells with both DGCs and PV-tdT+ basket cells using whole-cell patch-clamp recordings (Fig. 7*C*).

Surprisingly, AMPAR-mediated synaptic input onto PV-tdT+ cells was unaltered after SE [control = 61.2 ± 13.6 pA, $n = 13$ cells (8 mice), post-SE = 49.1 ± 10.7 pA, $n = 8$ cells (6 mice); Mann–Whitney, $p = 0.92$; Fig. 7*D*,*F*]. There was also no change in the paired pulse ratio [control = 1.50 ± 0.08 PPR, $n = 13$ cells (8 mice), post-SE = 1.49 ± 0.14 PPR, $n = 5$ cells (4 mice); Mann–Whitney, $p = 0.70$; Fig. 7*G*–*I*], suggesting that an increase in release probability at this synapse does not compensate for the reduction in the number of mossy cells post-SE.

To confirm that the maintained mossy cell-PV+ basket cell functional connectivity was not because of technical differences between the two different experimental approaches (Cre-dependent or Cre-independent vectors), or to potential variation in channelrhodopsin expression between animals, we made recordings from granule cells in the same slices as our PV-tdT+ recordings (either simultaneously or sequentially), while optogenetically stimulating the same set of contralateral mossy cell projections. Consistent with prior recordings, optogenetically-evoked excitatory (AMPAR-mediated) currents in DGCs were reduced after SE [control = 11.7 ± 2.1 pA, $n = 13$ cells (8 mice), post-SE = 5.3 ± 0.8 pA, $n = 8$ cells (6 mice); Mann–Whitney, $p = 0.0004$; Fig. 7*D*, *E*], demonstrating a selective loss of mossy-cell mediated inputs to DGCs compared with inputs to PV+ interneurons. The functionally preserved mossy cell-PV+ basket cell circuit, despite widespread mossy cell loss, suggests that the overall connectivity between the remaining mossy cells and target PV+ basket cells must increase to compensate and maintain overall excitatory drive of the PV+ interneuron network, which helps explain the relative preservation of mossy cell-meditated feedforward inhibition after SE.

Discussion

Hilar mossy cells form long-range bilateral projections in the hippocampus, and are the only intrinsic hippocampal inputs to provide widespread excitatory innervation of DGCs. Modification of mossy cell activity using chemogenetics is sufficient to alter learning tasks in mice (Bui et al., 2018), with others demonstrating the critical role of mossy cells in behavioral and memory tasks (Azevedo et al., 2019; Oh et al., 2020; Botterill et al., 2021b; Fredes and Shigemoto, 2021). These observations highlight the possible role of mossy cells in coordination and control of hippocampal functions, such as pattern separation in the dentate gyrus and DGC phase-locking (Soltesz et al., 1993; Buckmaster and Schwartzkroin, 1994;

Danielson et al., 2017; GoodSmith et al., 2017; Senzai and Buzsáki, 2017). Our results confirm that mossy cell loss in the pilocarpine model of TLE reduces overall excitatory connectivity between the mossy cell population and DGCs. Surprisingly, however, there also was a shift in the net output of the mossy cell network, with a relative preservation of mossy cell-mediated inhibitory tone in the dentate microcircuit. The maintained inhibitory tone reflects adaptive circuit plasticity post-SE and suggests that residual mossy cell activity could have anti-seizure effects in epilepsy.

Implications of mossy cell circuit plasticity for epileptogenesis

Mossy cell loss is a dominant feature of TLE in humans and in animal models (Nadler et al., 1980; Babb et al., 1984; Lowenstein et al., 1992; Obenaus et al., 1993; Blümcke et al., 2000), and has led to highly discussed hypotheses on its contribution to hippocampal hyperexcitability.

The first set of hypotheses on the role of mossy cell loss during epileptogenesis focused on excitatory connectivity between mossy cells and DGCs. Although one might expect that mossy cell loss would decrease excitatory input to DGCs, recordings of mossy cells in other disease models suggested that mossy cell loss was coincident with increased excitatory activation of the remaining mossy cells, and contributed to elevated excitation of DGCs (Santhakumar et al., 2000, 2005; Zhang et al., 2015). Taken together, these "irritable" mossy cells were hypothesized to drive dentate hyperexcitability and potentially contribute to seizure activity (Santhakumar et al., 2000; Ratzliff et al., 2002).

The alternative "dormant basket cell hypothesis" focused explicitly on the feedforward inhibitory component of the mossy cell circuit. This hypothesis was initially based on observations in slices from electrically kindled rats, in which granule cell hyperexcitability (i.e., multiple DGC population spikes after a single perforant path stimulus) was associated with mossy cell loss and decreased granule cell inhibition (Sloviter, 1991; Sloviter et al., 2003). An inability to drive paired-pulse inhibition in slices from epileptic animals led to the suggestion that loss of excitatory input from mossy cells may have rendered the remaining GABAergic basket cells "dormant." However, this interpretation has been controversial, as other studies have demonstrated that GABAergic hilar interneurons are also vulnerable to loss in other brain injury models (Santhakumar et al., 2000). Regardless, the dormant basket cell hypothesis suggested that mossy cell loss might contribute to epileptogenesis by reducing basket cell activation.

These two hypotheses were more recently examined in mice using two different strategies. Jinde et al. (2012) used transgenic mice to selectively express an inducible diphtheria toxin receptor in mossy cells. The specific ablation of almost all mossy cells did not cause spontaneous seizures or epilepsy when mice were followed for up to six weeks after ablation, although whole-cell patch-clamp recordings in DGCs demonstrated a transient hyperexcitability. These observations demonstrated that isolated mossy cell loss does not cause spontaneous seizures, and that the net effect of mossy cells, even in an epileptic brain, might be to reduce hippocampal hyperexcitability. Bui et al. (2018) used *in vivo* EEG recordings of seizures in a mouse model of TLE, while optogenetically activating or inactivating the surviving mossy cell population at the beginning of potential seizure-like discharges. Optogenetic activation of surviving mossy cells actually aborted seizures, whereas silencing mossy cells increased seizure frequency in these mice. Although these data do not neatly fit into the previous hypotheses, the elevated excitability of the dentate gyrus following mossy cell ablation (Jinde et al., 2012) and net anti-seizure effect of residual mossy cells in epilepsy (Bui et al., 2018) highlight the importance of mossy cells in inhibitory control of the dentate gyrus as proposed in the dormant basket cell hypothesis.

Consistent with these *in vivo* data, our results suggest a net inhibitory effect of residual mossy cell activity. However, adaptive

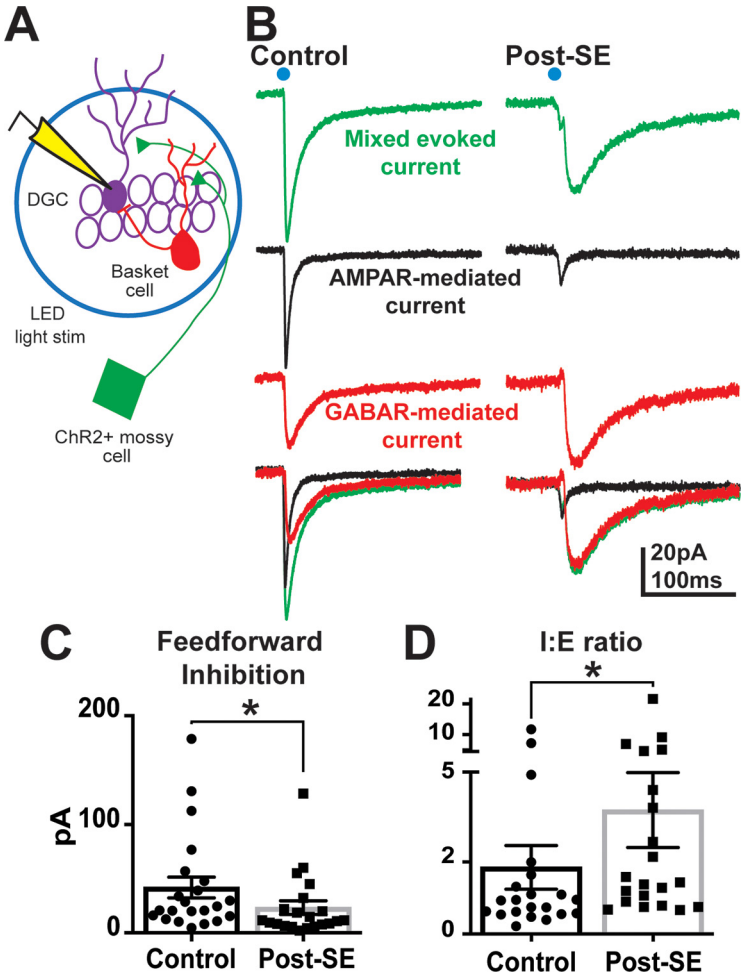

Figure 5. Relative preservation of mossy cell-driven feed-forward inhibition after mossy cell loss. ***A***, Schematic of the dentate mossy cell microcircuit, in which mossy cells (green) directly excite DGCs (purple) and also drive di-synaptic feed-forward inhibition via GABAergic interneurons, such as dentate basket cells (red). ***B***, Representative optogenetically-evoked mixed currents in DGCs (−70 mV, no drugs; green), as well as pharmacologically isolated, AMPAR-mediated currents (−70 mV w/10 μM SR95531; black), and GABAR-mediated (SR95531-sensitive; red) currents in DGCs from control and post-SE mice. ***C***, Summary data demonstrating reduced feedforward inhibition in DGCs from post-SE mice (*$p < 0.05$, Mann–Whitney). ***D***, The ratio of inhibition:excitation in DGCs after mossy cell activation is increased after SE, indicating relative preservation of feedforward inhibition after SE (*$p < 0.05$, Mann–Whitney).

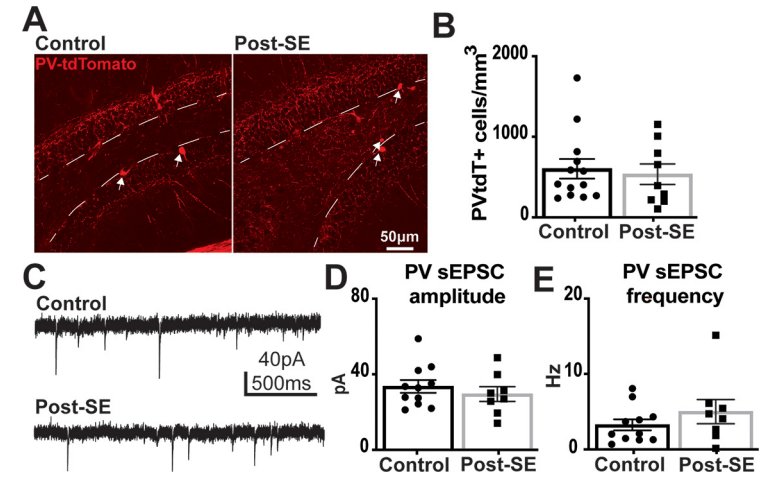

Figure 6. Cell density and spontaneous excitatory synaptic inputs onto PV+ basket cells are similar between control and post-SE mice. ***A***, Images of PV-tdT+ cells in the dentate gyrus of control and post-SE mice (dashed white line denotes the granule cell layer/hilus border and arrows indicate PV+ basket cells). ***B***, PV-tdT+ basket cell density is not different between control and post-SE mice ($p = 0.60$, Mann–Whitney). ***C***, Representative sEPSC recordings in PV-tdT+ cells from control and post-SE mice in the absence of light stimulation. ***D***, sEPSC amplitude in PV-tdT+ basket cells from control and post-SE mice is unaltered ($p = 0.45$, unpaired *t* test). ***E***, sEPSC frequency is similar in PV-tdT+ basket cells from control and post-SE mice, demonstrating that surviving PV-tdT+ basket cells are not dormant in post-SE mice ($p = 0.35$, Mann–Whitney).

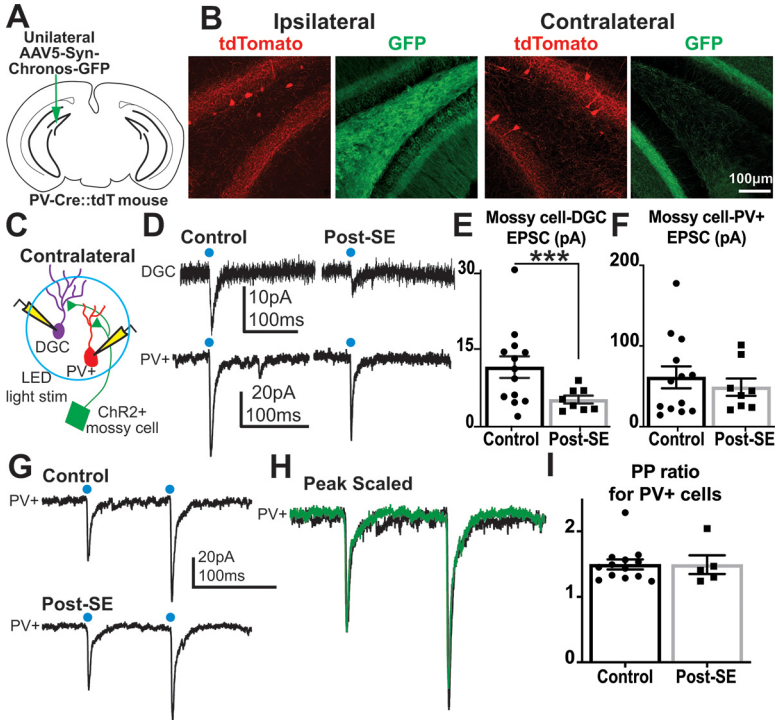

Figure 7. Overall mossy cell-driven excitation of PV+ basket cells is preserved despite mossy cell loss after SE ***A***, Schematic of unilateral channelrhodopsin (Chronos-GFP) virus injection in PV-Cre::tdTomato mice. ***B***, Images demonstrate Chronos-GFP expression (green) in the ipsilateral dentate and the contralateral IML, consistent with mossy cell expression. PV-tdT+ basket cells shown in red. ***C***, Schematic of the dual recording setup to test mossy cell connectivity onto DGCs and PV-tdT+ basket cells in PV-Cre::tdTomato mice. ***D***, Representative optogenetically-evoked EPSCs recorded from simultaneously-recorded PV-tdT+ basket cells and DGCs in control and post-SE mice. ***E***, Evoked mossy cell-DGC EPSC amplitudes in control and post-SE mice, demonstrating reduced amplitudes after SE (***$p < 0.001$, Mann–Whitney). ***F***, From the same slices assayed in panel ***E***, evoked mossy cell to PV-tdT+ EPSCs are not reduced after in post-SE mice ($p = 0.92$, Mann–Whitney). ***G***, Representative currents evoked by paired-pulse stimulation (100-ms interval) in PV-tdT+ basket cells from control and post-SE mice. ***H***, Peak-scaled responses from ***G***. ***I***, Paired pulse ratio is unchanged for mossy cell-evoked responses in PV-tdT+ basket cells from control and post-SE mice ($p = 0.70$, Mann–Whitney).

plasticity in the mossy cell-PV+ basket cell circuit demonstrates that basket cells are not as "dormant" as might be inferred by the degree of mossy cell loss. The net inhibitory output of the mossy cell circuit suggests that mossy cells may play an important role in maintaining inhibition of mature, neonatally-generated DGCs in the epileptic brain.

Although we did not observe increased mossy cell firing in post-SE mice, the reduced nature of circuits in a slice preparation might not accurately reflect patterns of mossy cell firing *in vivo*. The increased sEPSP frequency in surviving mossy cells after pilocarpine-induced SE does fit with the notion of "irritable" mossy cells, but this enhanced activation could serve to preserve inhibitory tone in the dentate microcircuit, as demonstrated with increased seizures when mossy cells are inhibited *in vivo* (Bui et al., 2018). Thus, perhaps mossy cells might be better described as "adaptable" rather than "irritable" in the epileptic hippocampal circuit.

Mossy cells also provide synaptic input onto immature DGCs, ectopically migrated granule cells, and semilunar granule cells in the IML (Williams et al., 2007; Chancey et al., 2014), and future studies examining how mossy cell loss affects these other excitatory neurons in the dentate could provide a more complete understanding of how mossy cell output impacts the overall dentate network function during epileptogenesis. Although we did not observe burst firing in mossy cells, higher frequency mossy cell firing might differentially recruit excitatory or inhibitory inputs, which could potentially be studied using optogenetic proteins with faster kinetics. Overall, a shift in the circuit balance to favor inhibition is reminiscent of reorganized inputs onto surviving inhibitory interneurons post-SE and after traumatic brain injury, which have been theorized to preserve circuit homeostasis in disease (Halabisky et al., 2010; Hunt et al., 2011; Butler et al., 2017).

Another important factor may also be the involvement of hilar mossy cells during both the initial insult and subsequent epileptogenesis following various brain injuries. Although our data are consistent with observations made from mice that had developed epilepsy (Bui et al., 2018), in which mossy cell activation had a net anti-seizure effect, a recent report demonstrated that chemogenetic inhibition of mossy cells before the induction of SE was sufficient to reduce overall seizure severity and progression to chronic epilepsy (Botterill et al., 2019). This observation would suggest that mossy cell activity may differentially engage

hippocampal circuits before, and likely during, epileptogenesis, particularly during the progression of structural and functional network changes involving progressive cell loss and axon rearrangement. During epileptogenesis, the onset of spontaneous seizures may contribute to further functional hippocampal circuit changes, and variability in the rate of progression toward epilepsy.

Mechanisms of mossy cell circuit plasticity

Preservation of feedforward inhibition onto DGCs despite significant mossy cell loss suggests that circuit plasticity may help maintain homeostasis after brain insults. Typically, circuit plasticity involves a combination of structural and functional adaptation. Strengthening of mossy cell-PV+ basket cell connections could be mediated through higher release probability, axon/terminal sprouting, or modification of postsynaptic receptors. The lack of change in paired pulse ratio in our experiments suggests that probability of release did not change. Thus, surviving mossy cells likely strengthen connections to target interneurons by either sprouting additional synapses or by strengthening of individual synapses. Axon sprouting by other principal neurons after brain injury contributes to increased excitatory innervation of interneurons (Halabisky et al., 2010; Hunt et al., 2011; Butler et al., 2017), and seems a candidate mechanism for preserved mossy cell-mediated feedforward inhibition. Additionally, mossy fiber sprouting into the IML occurs after brain insults and forms functional excitatory synapses onto DGCs (Hunt et al., 2010; Hendricks et al., 2017, 2019), although it is currently unclear whether these sprouted granule cell axons drive inhibitory basket cell function. Although we provide evidence for functional changes at the mossy cell-basket cell synapse, future studies could examine whether changes in the basket cell intrinsic properties such as the action potential threshold, or selective preservation of the coupling of specific sources of excitatory synaptic input to basket cell firing, might present additional opportunities for the homeostatic preservation of inhibition during epileptogenesis. Reduced interneuron excitability has been noted in other models of epilepsy (Tai et al., 2014); however, there have also been observations of impaired output of these interneurons onto target DGCs as well (Zhang and Buckmaster, 2009). Together, identification of the synaptic mechanisms underlying plasticity of the mossy cell–PV cell connections, as well as further analysis of the PV-DGC output properties, will be critical to fully understand how mossy cell loss in epilepsy impacts dentate circuit function in disease.

Future work determining the mechanisms that underlie the selective plasticity for mossy cell-PV+ basket cell synapses, as well as the potential involvement of other interneuron subtypes including nonbasket cells, will be important to determine how generally applicable these circuit changes are after various brain insults (i.e., traumatic brain injury and stroke), and if the enhancement of this adaptive plasticity could be a promising therapeutic strategy to increase inhibition of DGCs in epilepsy, thus reducing dentate hyperexcitability and, hopefully, seizures.

References

Azevedo EP, Pomeranz L, Cheng J, Schneeberger M, Vaughan R, Stern SA, Tan B, Doerig K, Greengard P, Friedman JM (2019) A role of Drd2 hippocampal neurons in context-dependent food intake. Neuron 102:873–886.e5.

Babb TL, Brown WJ, Pretorius J, Davenport C, Lieb JP, Crandall PH (1984) Temporal lobe volumetric cell densities in temporal lobe epilepsy. Epilepsia 25:729–740.

Blümcke I, Suter B, Behle K, Kuhn R, Schramm J, Elger C, Wiestler O (2000) Loss of hilar mossy cells in Ammon's horn sclerosis. Epilepsia 41:S174–S180.

Borges K, Gearing M, McDermott DL, Smith AB, Almonte AG, Wainer BH, Dingledine R (2003) Neuronal and glial pathological changes during epileptogenesis in the mouse pilocarpine model. Exp Neurol 182:21–34.

Botterill JJ, Lu YL, LaFrancois JJ, Bernstein HL, Alcantara-Gonzalez D, Jain S, Leary P, Scharfman HE (2019) An excitatory and epileptogenic effect of dentate gyrus mossy cells in a mouse model of epilepsy. Cell Rep 29:2875–2889.e6.

Botterill JJ, Gerencer KJ, Vinod KY, Alcantara-Gonzalez D, Scharfman HE (2021a) Dorsal and ventral mossy cells differ in their axonal projections throughout the dentate gyrus of the mouse hippocampus. Hippocampus 31:522–539.

Botterill JJ, Vinod KY, Gerencer KJ, Teixeira CM, LaFrancois JJ, Scharfman HE (2021b) Bidirectional regulation of cognitive and anxiety-like behaviors by dentate gyrus mossy cells in male and female mice. J Neurosci 41:2475–2495.

Botterill JJ, Khlaifia A, Walters BJ, Brimble MA, Scharfman HE, Arruda-Carvalho M (2021c) Off-Target expression of Cre-dependentt adeno-associatted viruses in wild-type C57BL/6J mice. eNeuro 8:ENEURO.0363-21.2021.

Brooks-Kayal AR, Shumate MD, Jin H, Rikhter TY, Coulter DA (1998) Selective changes in single cell GABA A receptor subunit expression and function in temporal lobe epilepsy. Nat Med 4:1166–1172.

Buckmaster PS, Schwartzkroin PA (1994) Hippocampal mossy cell function: a speculative view. Hippocampus 4:393–402.

Buckmaster PS, Dudek FE (1997) Neuron loss, granule cell axon reorganization, and functional changes in the dentate gyrus of epileptic kainate-treated rats. J Comp Neurol 385:385–404.

Buckmaster PS, Haney MM (2012) Factors affecting outcomes of pilocarpine treatment in a mouse model of temporal lobe epilepsy. Epilepsy Res 102:153–159.

Buckmaster PS, Wenzel HJ, Kunkel DD, Schwartzkroin PA (1996) Axon arbors and synaptic connections of hippocampal mossy cells in the rat in vivo. J Comp Neurol 366:270–292.

Buckmaster PS, Abrams E, Wen X (2017) Seizure frequency correlates with loss of dentate gyrus GABAergic neurons in a mouse model of temporal lobe epilepsy. J Comp Neurol 525:2592–2610.

Bui AD, Nguyen TM, Limouse C, Kim HK, Szabo GG, Felong S, Maroso M, Soltesz I (2018) Dentate gyrus mossy cells control spontaneous convulsive seizures and spatial memory. Science 359:787–790.

Burger C, Gorbatyuk OS, Velardo MJ, Peden CS, Williams P, Zolotukhin S, Reier PJ, Mandel RJ, Muzyczka N (2004) Recombinant AAV viral vectors pseudotyped with viral capsids from serotypes 1, 2, and 5 display differential efficiency and cell tropism after delivery to different regions of the central nervous system. Mol Ther 10:302–317.

Butler CR, Boychuk JA, Smith BN (2017) Brain injury-induced synaptic reorganization in hilar inhibitory neurons is differentially suppressed by rapamycin. eNeuro 4:ENEURO.0134-17.2017.

Castle MJ, Gershenson ZT, Giles AR, Holzbaur EL, Wolfe JH (2014) Adeno-associated virus serotypes 1, 8, and 9 share conserved mechanisms for anterograde and retrograde axonal transport. Hum Gene Ther 25:705–720.

Chancey JH, Poulsen DJ, Wadiche JI, Overstreet-Wadiche L (2014) Hilar mossy cells provide the first glutamatergic synapses to adult-born dentate granule cells. J Neurosci 34:2349–2354.

Danielson NB, Turi GF, Ladow M, Chavlis S, Petrantonakis PC, Poirazi P, Losonczy A (2017) In vivo imaging of dentate gyrus mossy cells in behaving mice. Neuron 93:552–559.e4.

De Lanerolle N, Kim J, Robbins RJ, Spencer D (1989) Hippocampal interneuron loss and plasticity in human temporal lobe epilepsy. Brain Res 495:387–395.

Fredes F, Shigemoto R (2021) The role of hippocampal mossy cells in novelty detection. Neurobiol Learn Mem 183:107486.

GoodSmith D, Chen X, Wang C, Kim SH, Song H, Burgalossi A, Christian KM, Knierim JJ (2017) Spatial representations of granule cells and mossy cells of the dentate gyrus. Neuron 93:677–690.e5.

Gupta A, Elgammal FS, Proddutur A, Shah S, Santhakumar V (2012) Decrease in tonic inhibition contributes to increase in dentate semilunar granule cell excitability after brain injury. J Neurosci 32:2523–2537.

Halabisky B, Parada I, Buckmaster PS, Prince DA (2010) Excitatory input onto hilar somatostatin interneurons is increased in a chronic model of epilepsy. J Neurophysiol 104:2214–2223.

Hashimotodani Y, Nasrallah K, Jensen KR, Chávez AE, Carrera D, Castillo PE (2017) LTP at hilar mossy cell-dentate granule cell synapses modulates dentate gyrus output by increasing excitation/inhibition balance. Neuron 95:928–943.e3.

Hendricks WD, Chen Y, Bensen AL, Westbrook GL, Schnell E (2017) Short-term depression of sprouted mossy fiber synapses from adult-born granule cells. J Neurosci 37:5722–5735.

Hendricks WD, Westbrook GL, Schnell E (2019) Early detonation by sprouted mossy fibers enables aberrant dentate network activity. Proc Natl Acad Sci USA 116:10994–10999.

Hippenmeyer S, Vrieseling E, Sigrist M, Portmann T, Laengle C, Ladle DR, Arber S (2005) A developmental switch in the response of DRG neurons to ETS transcription factor signaling. PLoS Biol 3:e159.

Houser CR, Peng Z, Wei X, Huang CS, Mody I (2020) Mossy cells in the dorsal and ventral dentate gyrus differ in their patterns of axonal projections. J Neurosci 41:991–1004.

Hsu TT, Lee CT, Tai MH, Lien CC (2016) Differential recruitment of dentate gyrus interneuron types by commissural versus perforant pathways. Cereb Cortex 26:2715–2727.

Hunt RF, Scheff SW, Smith BN (2010) Regionally localized recurrent excitation in the dentate gyrus of a cortical contusion model of posttraumatic epilepsy. J Neurophysiol 103:1490–1500.

Hunt RF, Scheff SW, Smith BN (2011) Synaptic reorganization of inhibitory hilar interneuron circuitry after traumatic brain injury in mice. J Neurosci 31:6880–6890.

Jiao Y, Nadler JV (2007) Stereological analysis of GluR2-immunoreactive hilar neurons in the pilocarpine model of temporal lobe epilepsy: correlation of cell loss with mossy fiber sprouting. Exp Neurol 205:569–582.

Jinde S, Zsiros V, Jiang Z, Nakao K, Pickel J, Kohno K, Belforte JE, Nakazawa K (2012) Hilar mossy cell degeneration causes transient dentate granule cell hyperexcitability and impaired pattern separation. Neuron 76:1189–1200.

Larimer P, Strowbridge BW (2008) Nonrandom local circuits in the dentate gyrus. J Neurosci 28:12212–12223.

Lowenstein DH, Thomas MJ, Smith DH, McIntosh TK (1992) Selective vulnerability of dentate hilar neurons following traumatic brain injury: a potential mechanistic link between head trauma and disorders of the hippocampus. J Neurosci 12:4846–4853.

Luikart BW, Schnell E, Washburn EK, Bensen AL, Tovar KR, Westbrook GL (2011) Pten knockdown in vivo increases excitatory drive onto dentate granule cells. J Neurosci 31:4345–4354.

Madisen L, et al. (2012) A toolbox of Cre-dependent optogenetic transgenic mice for light-induced activation and silencing. Nat Neurosci 15:793–802.

Mello LE, Cavalheiro EA, Tan AM, Kupfer WR, Pretorius JK, Babb TL, Finch DM (1993) Circuit mechanisms of seizures in the pilocarpine model of chronic epilepsy: cell loss and mossy fiber sprouting. Epilepsia 34:985–995.

Nadler JV (2003) The recurrent mossy fiber pathway of the epileptic brain. Neurochem Res 28:1649–1658.

Nadler JV, Perry BW, Cotman CW (1980) Selective reinnervation of hippocampal area CA1 and the fascia dentata after destruction of CA3-CA4 afferents with kainic acid. Brain Res 182:1–9.

Obenaus A, Esclapez M, Houser C (1993) Loss of glutamate decarboxylase mRNA-containing neurons in the rat dentate gyrus following pilocarpine-induced seizures. J Neurosci 13:4470–4485.

Oh SJ, Cheng J, Jang JH, Arace J, Jeong M, Shin CH, Park J, Jin J, Greengard P, Oh YS (2020) Hippocampal mossy cell involvement in behavioral and neurogenic responses to chronic antidepressant treatment. Mol Psychiatry 25:1215–1228.

Racine RJ (1972) Modification of seizure activity by electrical stimulation: II. Motor seizures. Electrorencephalogr. Clin. Neurophysiol 32:281–294.

Ratzliff A, Santhakumar V, Howard A, Soltesz I (2002) Mossy cells in epilepsy: rigor mortis or vigor mortis? Trends Neurosci 25:140–144.

Ribak CE, Seress L (1983) Five types of basket cell in the hippocampal dentate gyrus: a combined Golgi and electron microscopic study. J Neurocytol 12:577–597.

Rovira-Esteban L, Hájos N, Nagy GA, Crespo C, Nacher J, Varea E, Blasco-Ibáñez JM (2020) Semilunar granule cells are the primary source of the perisomatic excitatory innervation onto parvalbumin-expressing interneurons in the dentate gyrus. eNeuro 7: ENEURO.0323-19.2020.

Santhakumar V, Bender R, Frotscher M, Ross ST, Hollrigel GS, Toth Z, Soltesz I (2000) Granule cell hyperexcitability in the early post-traumatic rat dentate gyrus: the 'irritable mossy cell' hypothesis. J Physiol 524:117–134.

Santhakumar V, Aradi I, Soltesz I (2005) Role of mossy fiber sprouting and mossy cell loss in hyperexcitability: a network model of the dentate gyrus incorporating cell types and axonal topography. J Neurophysiol 93:437–453.

Save L, Baude A, Cossart R (2019) Temporal embryonic origin critically determines cellular physiology in the dentate gyrus. Cereb Cortex 29:2639–2652.

Scharfman HE (1994a) EPSPs of dentate gyrus granule cells during epileptiform bursts of dentate hilar "mossy" cells and area CA3 pyramidal cells in disinhibited rat hippocampal slices. J Neurosci 14:6041–6057.

Scharfman HE (1994b) Evidence from simultaneous intracellular recordings in rat hippocampal slices that area CA3 pyramidal cells innervate dentate hilar mossy cells. J Neurophysiol 72:2167–2180.

Scharfman HE (1995) Electrophysiological evidence that dentate hilar mossy cells are excitatory and innervate both granule cells and interneurons. J Neurophysiol 74:179–194.

Scharfman HE (2007) The CA3 "backprojection" to the dentate gyrus. Prog Brain Res 163:627–637.

Scharfman HE (2016) The enigmatic mossy cell of the dentate gyrus. Nat Rev Neurosci 17:562–575.

Scharfman HE, Myers CE (2013) Hilar mossy cells of the dentate gyrus: a historical perspective. Front Neural Circuits 6:106.

Schiffmann SN, Cheron G, Lohof A, d'Alcantara P, Meyer M, Parmentier M, Schurmans S (1999) Impaired motor coordination and Purkinje cell excitability in mice lacking calretinin. Proc Natl Acad Sci USA 96:5257–5262.

Senzai Y, Buzsáki G (2017) Physiological properties and behavioral correlates of hippocampal granule cells and mossy cells. Neuron 93:691–704.e5.

Shibley H, Smith BN (2002) Pilocarpine-induced status epilepticus results in mossy fiber sprouting and spontaneous seizures in C57BL/6 and CD-1 mice. Epilepsy Res 49:109–120.

Sloviter RS (1987) Decreased hippocampal inhibition and a selective loss of interneurons in experimental epilepsy. Science 235:73–76.

Sloviter RS (1991) Permanently altered hippocampal structure, excitability, and inhibition after experimental status epilepticus in the rat: the "dormant basket cell" hypothesis and its possible relevance to temporal lobe epilepsy. Hippocampus 1:41–66.

Sloviter RS, Zappone CA, Harvey BD, Bumanglag AV, Bender RA, Frotscher M (2003) "Dormant basket cell" hypothesis revisited: relative vulnerabilities of dentate gyrus mossy cells and inhibitory interneurons after hippocampal status epilepticus in the rat. J Comp Neurol 459:44–76.

Soltesz I, Bourassa J, Deschênes M (1993) The behavior of mossy cells of the rat dentate gyrus during theta oscillations in vivo. Neuroscience 57:555–564.

Soriano E, Frotscher M (1989) A GABAergic axo-axonic cell in the fascia dentata controls the main excitatory hippocampal pathway. Brain Res 503:170–174.

Sun Y, Grieco SF, Holmes TC, Xu X (2017) Local and long-range circuit connections to hilar mossy cells in the dentate gyrus. eNeuro 4:ENEURO.0097-17.2017.

Tai C, Abe Y, Westenbroek RE, Scheuer T, Catterall WA (2014) Impaired excitability of somatostatin- and parvalbumin-expressing cortical interneurons in a mouse model of Dravet syndrome. Proc Natl Acad Sci USA 111:E3139–E3148.

Tovar KR, Westbrook GL (1999) The incorporation of NMDA receptors with a distinct subunit composition at nascent hippocampal synapses in vitro. J Neurosci 19:4180–4188.

Tovar KR, Sprouffske K, Westbrook GL (2000) Fast NMDA receptor-mediated synaptic currents in neurons from mice lacking the epsilon2 (NR2B) subunit. J Neurophysiol 83:616–620.

Vaden RJ, Gonzalez JC, Tsai MC, Niver AJ, Fusilier AR, Griffith CM, Kramer RH, Wadiche JI, Overstreet-Wadiche L (2020) Parvalbumin interneurons provide spillover to newborn and mature dentate granule cells. Elife 9:e54125.

Varea E, Nácher J, Blasco-Ibáñez JM, Gómez-Climent MA, Castillo-Gómez E, Crespo C, Martínez-Guijarro FJ (2005) PSA-NCAM expression in the rat medial prefrontal cortex. Neuroscience 136:435–443.

Williams PA, Larimer P, Gao Y, Strowbridge BW (2007) Semilunar granule cells: glutamatergic neurons in the rat dentate gyrus with axon collaterals in the inner molecular layer. J Neurosci 27:13756–13761.

Winokur RS, Kubal T, Liu D, Davis SF, Smith BN (2004) Recurrent excitation in the dentate gyrus of a murine model of temporal lobe epilepsy. Epilepsy Res 58:93–105.

Wittner L, Maglóczky Z, Borhegyi Z, Halász P, Tóth S, Eross L, Szabó Z, Freund TF (2001) Preservation of perisomatic inhibitory input of granule cells in the epileptic human dentate gyrus. Neuroscience 108:587–600.

Zhang W, Buckmaster PS (2009) Dysfunction of the dentate basket cell circuit in a rat model of temporal lobe epilepsy. J Neurosci 29:7846–7856.

Zhang W, Thamattoor AK, LeRoy C, Buckmaster PS (2015) Surviving mossy cells enlarge and receive more excitatory synaptic input in a mouse model of temporal lobe epilepsy. Hippocampus 25:594–604.